Density Functional Theory Study of the Structures and Properties of $(H_2AlN_3)_n$ ($n = 1-4$) Clusters

Qi Ying Xia, He Ming Xiao,* Xue Hai Ju, and Xue Dong Gong

Department of Chemistry, Nanjing University of Science and Technology, Nanjing, 210094, People's Republic of China

Received: September 4, 2003; In Final Form: January 6, 2004

The DFT/B3LYP method with different basis sets has been applied to the systems of $(H_2AlN_3)_n$ ($n = 1-4$). $(H_2AlN_3)_2$ is found to exhibit the planar Al_2N_2 ring structure and possesses D_{2h} symmetry. The transition state for the monomer to dimer conversion is located, and the activation energy is presented. $(H_2AlN_3)_3$ involving a six-membered Al_3N_3 ring is found to exhibit two minima with very similar binding energies (ca. −274 to −278 kJ·mol^{-1}). One minimum found possesses C_s symmetry and displays boatlike conformation. Another minimum found possesses C_{3v} symmetry with chairlike conformation. $(H_2AlN_3)_4$ occurs in several structures with Al_4N_4 eight-membered ring structures that correspond to the minima with slight energy differences among them. Compared to the monomer, both the structural changes and charge transfers for the clusters are large. Frequency calculations are carried out on each optimized structure, and their IR spectra are discussed. Thermodynamic properties reveal the system of H_2AlN_3 is involved in dimer−trimer−tetramer equilibria, and the trimer is the main component.

1. Introduction

The inorganic and organoaluminum azide compounds have been widely used in many fields. These compounds are used as the azidating agents, and the energetic materials which are used in national defense industries and in space technology, especially to generate thin films of AlN in various chemical vapor deposition (CVD) systems.[1,2] Aluminum nitride has useful properties for coatings, especially for optical or optoelectronic devices, acoustic wave devices, and electronic microcircuits.[3]

Recently, McMurran et al.[4,5] have reported the development of a simple and highly efficient approach for growing GaN thin films using the newly synthesized molecular source H_2GaN_3. H_2GaN_3 is a volatile and highly reactive compound and is particularly attractive as a CVD source because it can eliminate extremely stable H_2 and N_2 byproducts to yield pure and stoichiometric GaN very effectively at low temperatures. From the experimental point of view, Al is chosen as the metal center to be considered in the present investigation because it is a p-block metal, valence isoelectronic with Ga, but the availability, low cost, and stability of Al make it an attractive candidate. From the computational point of view, Al is lighter than Ga, so calculations involving Al are simpler and computationally less demanding than calculations on Ga. It is known that the relative energies and other computed properties will change at the multireference level. In this paper we only employ density functional theory (DFT) at the B3LYP level with different basis sets to predict the characters of the new $(H_2AlN_3)_n$ with n up to 4, including the stable optimized geometries, binding energies, and IR spectra. The thermodynamic properties, in particular, can provide useful information for the synthesis of $(H_2AlN_3)_{2-4}$. Another aim of this work is to choose an appropriate basis set for an accurate description of the similar systems.

* Corresponding author. Fax: +86-25-84431622. E-mail: xiao@mail.njust.edu.cn.

2. Methods

The H_2AlN_3 monomer and all its possible stable clusters obtained from ChemBats3D software were fully optimized by the Berny method at the B3LYP level at different basis sets.[6−8] Vibrational frequencies calculated show that each structure is characterized to be a stable structure (no imaginary frequencies).

For the following intermolecular interaction

$$n H_2AlN_3 \rightarrow (H_2AlN_3)_n \quad (n = 2-4) \tag{1}$$

the binding energy (ΔE) of the complex is determined as

$$\Delta E = E_n - nE_1 \quad (n = 2-4) \tag{2}$$

where E_n and E_1 are the total energies of clusters $(H_2AlN_3)_{2-4}$ and the isolated H_2AlN_3, respectively.

As is well-known, it is important to choose an appropriate basis set for an accurate description of the structures and energies of clusters. Usually a substantial size of basis set is required; however, the size of the clusters studied in this work excluded the use of a very large basis set, and hence we employed the 6-311+G* basis set to study $(H_2AlN_3)_n$ with n up to 4, which had been successfully applied to Al_2N_4 and AlN_n ($n = 4-7$) systems.[9] To ensure the adequacy of this basis set, we also computed the H_2AlN_3 monomer and $(H_2AlN_3)_2$ dimer with the 6-311++G** and aug-cc-pVTZ basis sets. As shown later on, the results obtained from all basis sets were quite similar except for slight numerical differences. The energies for the dimer and monomer were also evaluated using the single-point CCSD(T)/6-311+G* method at the B3LYP/6-311+G* geometries with inclusion of the B3LYP/6-311+G* zero-point vibration energies.

All calculations were carried out with the Gaussian98 program[10] on a Pentium- computer using the default convergence criteria.

10.1021/jp0310450 CCC: $27.50
Published on Web 03/17/2004

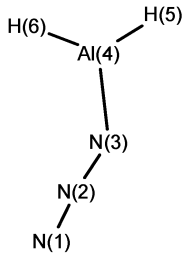

1A

Figure 1. Minimum of H_2AlN_3 monomer.

TABLE 1: Geometry of H_2AlN_3 Monomer As Optimized at the B3LYP Level with Different Basis Sets (Bond lengths in Angstroms; Angles in Degrees; See Figure 1 for Numbering)

	6-311+G*	6-311++G**	aug-cc-pVTZ
N(1)−N(2)	1.135	1.135	1.130
N(2)−N(3)	1.212	1.212	1.211
N(3)−Al(4)	1.803	1.803	1.798
Al(4)−H(5)	1.569	1.568	1.567
Al(4)−H(6)	1.576	1.575	1.575
N(1)−N(2)−N(3)	176.2	176.2	176.2
N(2)−N(3)−Al(4)	140.8	140.7	137.9
N(3)−Al(4)−H(5)	114.7	114.7	114.6
N(3)−Al(4)−H(6)	118.8	118.7	119.2
H(5)−Al(4)−H(6)	126.5	126.5	126.2
N(1)−N(2)−N(3)−Al(4)	180.0	180.0	178.8
N(2)−N(3)−Al(4)−H(5)	180.0	180.0	180.0
N(2)−N(3)−Al(4)−H(6)	0.0	0.0	0.0

3. Results and Discussions

This section presents and discusses the results, including geometric features, charge distribution, stability, vibrations, and thermodynamic properties obtained in the theoretical study of H_2AlN_3 and its clusters. The results of the geometric features for H_2AlN_3 and $(H_2AlN_3)_2$ are discussed first and used to assess the quality of the basis set used.

TABLE 2: Geometry of $(H_2AlN_3)_2$ Dimer As Optimized at the B3LYP Level with Different Basis Sets (the Same Values Are Omitted; Bond Lengths in Angstroms; Angles in Degrees; See Figure 2 for Numbering)

	6-311+G*	6-311++G**	aug-cc-pVTZ
N(1)−N(2)	1.128	1.128	1.123
N(2)−N(3)	1.228	1.228	1.225
N(3)−Al(4)	1.985	1.984	1.973
Al(4)−H(5)	1.579	1.579	1.578
N(1)−N(2)−N(3)	180.0	180.0	180.0
N(2)−N(3)−Al(4)	129.8	129.8	130.0
Al(4)−N(3)−Al(10)	100.3	100.4	100.1
N(3)−Al(4)−N(9)	79.7	79.7	79.9
N(3)−Al(4)−H(5)	111.2	111.2	111.2
H(5)−Al(4)−H(6)	123.8	123.8	123.7
N(1)−N(2)−N(3)−Al(4)	0.0	0.0	0.0
N(2)−N(3)−Al(4)−H(5)	−71.1	−71.1	−71.0
Al(10)−N(3)−Al(4)−N(9)	0.0	0.0	0.0
Al(10)−N(3)−Al(4)−H(5)	108.9	108.9	109.0
N(2)−N(3)−Al(10)−N(9)	180.0	180.0	180.0

(3.1) Geometries. *(3.1.1) H_2AlN_3 Monomer.* Table 1 lists the geometric results for the H_2AlN_3 monomer obtained by using the DFT/B3LYP method with different basis sets, and Figure 1 shows the structure obtained.

The optimized geometry possesses C_s symmetry in all instances. The N−N−N bond angle is about 176.2°. There are two distinct N−N distances within the azide group, with the shorter one corresponding to the terminal N−N bond (1.13 Å). The results obtained using the 6-311+G*, 6-311++G**, and aug-cc-pVTZ basis sets at the B3LYP level are similar, and the bond lengths obtained with the aug-cc-pVTZ basis set are slightly shorter than those obtained with the 6-311+G* and 6-311++G** basis sets. However, ensuring accurate estimates of these quantities entails using a large basis set and makes computations on the large $(H_2AlN_3)_4$ impractical. For this reason, and on the basis of the results for the $(H_2AlN_3)_2$ discussed in the following section, we chose to adopt the 6-311+G* basis set for computations on the larger systems of $(H_2AlN_3)_3$ and $(H_2AlN_3)_4$.

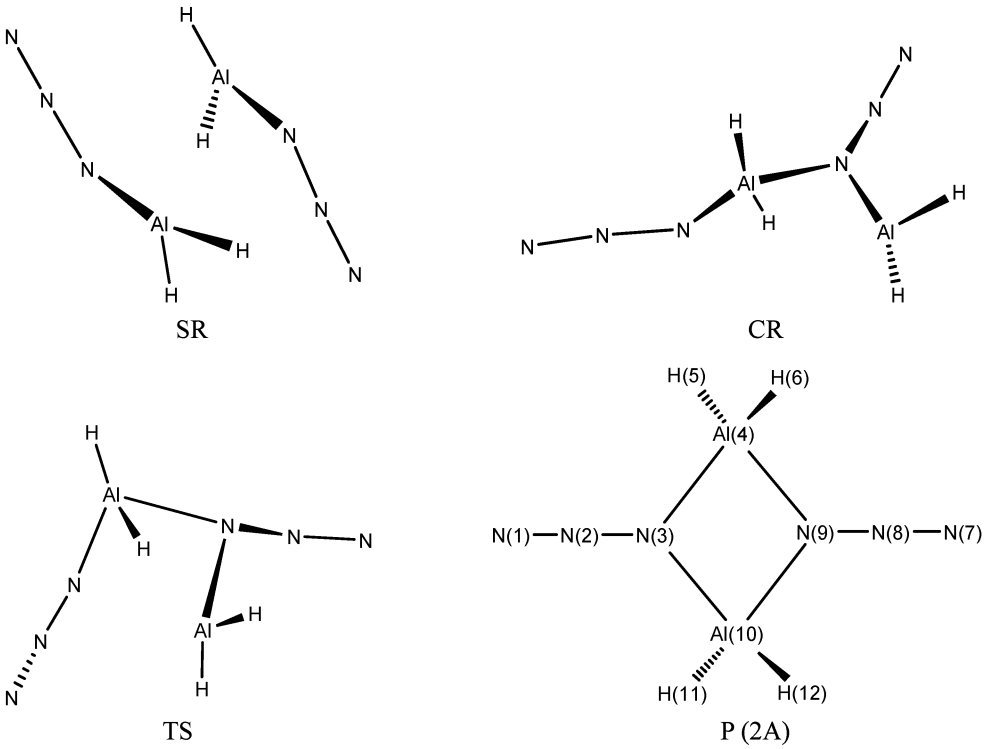

Figure 2. Molecular structures of the separated reactant (SR), the complex of reactant (CR), the transition state (TS), and product (P).

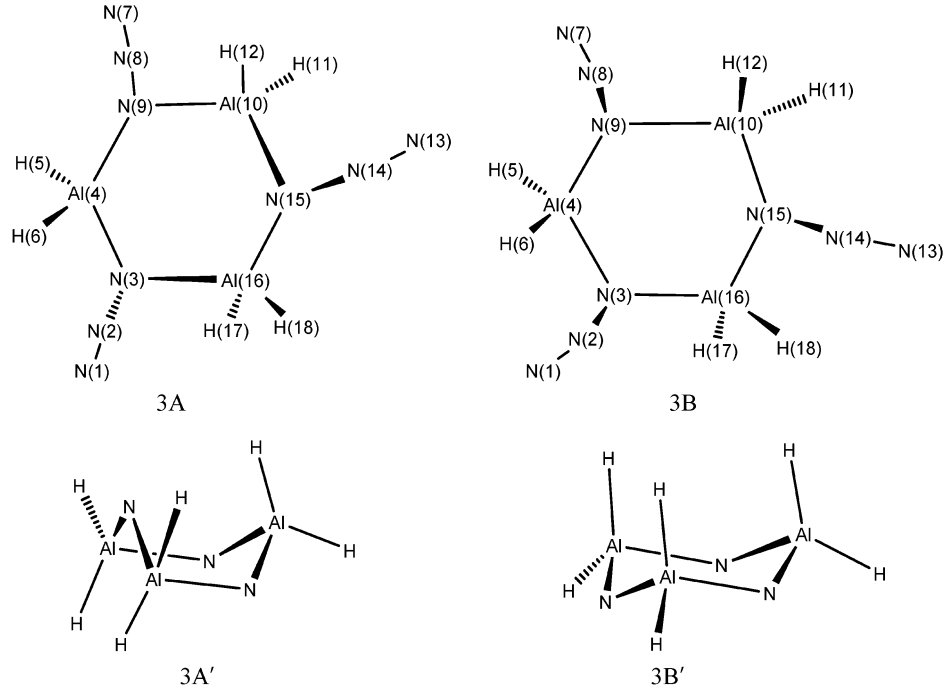

Figure 3. Molecular structures of $(H_2AlN_3)_3$ displaying boat and chair conformations.

(3.1.2) $(H_2AlN_3)_2$ Dimer. Our computational method and basis sets derived the stable structure 2A shown in Figure 2. The structural parameters obtained are summarized in Table 2. The $(H_2AlN_3)_2$ dimer consists of two monomer units, each linked by the α-nitrogen of the azide group (connectivity: $H_2Al-N_\alpha-N_\beta-N_\gamma$). It has been previously established that in the polymeric I_2GaN_3 [11] and $[Cl_2InN_3(THF)_2]_2$ [12] (THF = tetrahydrofuran) compounds, cross-linking of the Ga or In atoms occurs via the α-nitrogen of the N_3 ligands. On the other hand, the $N_3In-[(CH_2)_3NMe_2]_2$ [13] compound forms a polymeric structure in which cross-linking of the In atoms occurs via the γ-nitrogen of the N_3 ligand.

Our computational results of the gas-phase structure reveal dimeric units containing an Al−N−Al linkage rather than the Al−N−N−N−Al linkage similar to the In−N−In linkage, rather than the In−N−N−N−In linkage which occurs in the liquid-state structure of $[(C_2H_5)_2InN_3]_2$ [14] and in the solid-state structure of $[Cl_2InN_3(THF)_2]_2$.[12]

The Al_2N_2 tetragonal framework has not been previously established in the structures of inorganic and organoaluminum azides. Nevertheless, such a planar, four-membered structure has been proposed for the dimeric azide of the indium complex, $[(C_2H_5)_2InN_3]_2$,[14] and similar In_2N_2 rings have been found in the structures of organometallic amides of indium[15] and $[Cl_2InN_3(THF)_2]_2$.[12]

The optimized geometry possesses D_{2h} symmetry in all instances. The results obtained from different basis sets are generally in agreement, with bond lengths from the aug-cc-pVTZ basis set being slightly shorter than those from the other two basis sets used. This shows that it is appropriate to choose the 6-311+G* basis set to compute the $(H_2AlN_3)_3$ and $(H_2AlN_3)_4$ systems. So in this work we only report the change of bond lengths between the monomer and dimer with the 6-311+G* basis set. The bond lengths N(α)−Al(1.985 Å) all increase by 18.2 pm. N(α)−N(β) bond lengths (1.228 Å) in the dimeric structure both increase by 1.6 pm; however, N(β)−N(γ) bond lengths (1.128 Å) both decrease by 0.7 pm. The N−N−N bond angles are 180.0°, which is typical of those reported for other crystalline group 13 covalent azides. The average bond angles for N−N−Al, N−Al−N, and Al−N−Al are ca. 130.0, 80.0, and 100.0°, respectively. Obviously, the geometric parameters of $(H_2AlN_3)_2$ change considerably compared with those of the monomer.

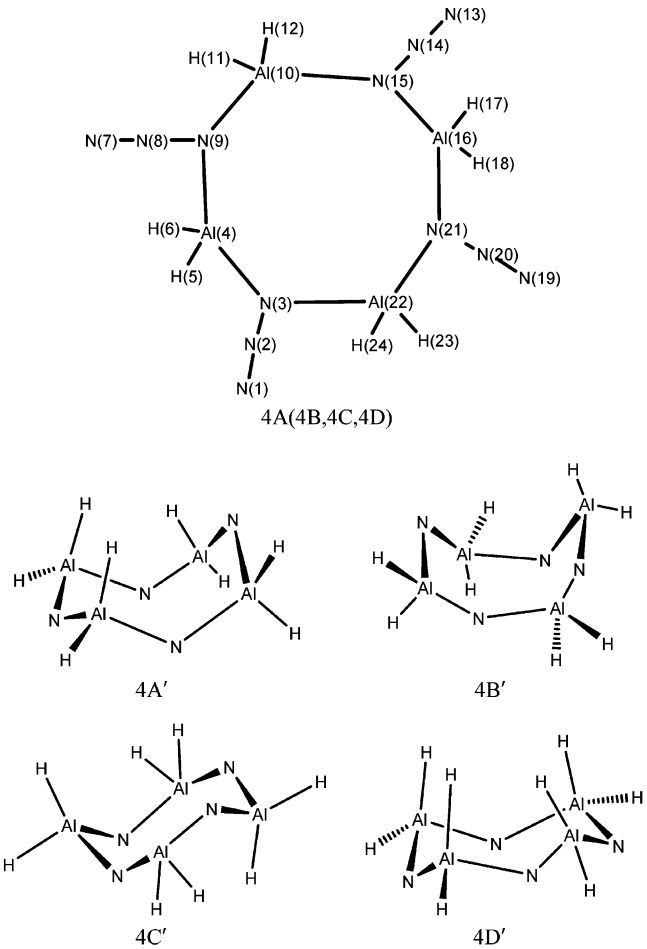

Figure 4. Molecular structures of $(H_2AlN_3)_4$ displaying Al_4N_4 ring structures.

TABLE 3: Energies of the H_2AlN_3 Clusters and the Transition State

	E	ΔE	ZPE	ΔE_{ZPEC}	E_{HOMO}	E_{LUMO}	E_{gap}
1A	−1 071 001.10		69.86		−0.29	−0.08	0.21
1A[a]	−1 071 006.15		69.81		−0.29	−0.08	0.21
1A[b]	−1 071 067.63		69.98		−0.29	−0.08	0.21
1A[c]	−1 068 661.97		69.86				
SR	−2 142 002.20		139.72				
SR[c]	−2 137 323.94		139.72				
CR	−2 142 136.68		150.99				
CR[c]	−2 137 484.38		150.99				
TS	−2 142 068.46		148.04				
TS[c]	−2 137 420.41		148.04				
2A	−2 142 177.96	−175.76	149.27	−166.60	−0.29	−0.07	0.22
2A[a]	−2 142 188.15	−175.85	149.20	−166.65	−0.29	−0.07	0.22
2A[b]	−2 142 306.48	−171.22	148.71	−162.83	−0.29	−0.07	0.22
2A[c]	−2 137 531.98	−208.04	149.27	−198.87			
3A	−3 213 297.99	−294.69	227.06	−277.91	−0.30	−0.07	0.23
3B	−3 213 293.85	−290.55	226.60	−274.21	−0.31	−0.07	0.24
4A	−4 284 407.37	−402.97	303.94	−379.45	−0.30	−0.07	0.23
4B	−4 284 402.74	−398.34	304.11	−374.66	−0.31	0.09	0.22
4C	−4 284 401.85	−397.45	303.81	−374.05	−0.30	−0.08	0.22
4D	−4 284 399.42	−395.01	303.75	−371.67	−0.30	−0.07	0.23

[a−c] Data are from the B3LYP/6-311++G**, B3LYP/aug-cc-pVTZ, and CCSD(T)/ 6-311+G* levels, respectively. The rest of the data are from B3LYP/6-311+G*. E, ZPE, ΔE, and ΔE_{ZPEC} are the total energy, zero-point energy, and uncorrected and corrected binding energies (kJ·mol^{-1}), respectively. E_{HOMO}, E_{LUMO}, and E_{gap} are the energies of the HOMO, LUMO, and their gap (au).

Figure 2 also gives a transition-state (TS) structure and a complex of reactant (CR) fully optimized at the B3LYP/6-311+G* level and the separated reactant (SR). Intrinsic reaction coordinate (IRC) calculations were carried out at the same level to confirm that the transition state connects the reactant and product.

(3.1.3) $(H_2AlN_3)_3$ Trimer. Figure 3 shows the minima located for the $(H_2AlN_3)_3$ trimer (structures 3A and 3B); the N_2 portion of the N_3 group is omitted for clarity reasons from these figures to give Figure 3A′,B′. Our computation reveals two types of trimer $(H_2AlN_3)_3$: a boatlike conformation 3A (symmetric C_s) and a chairlike conformation 3B (symmetric C_{3v}). Both of these possess an Al molecular ring system formed by means of bridged azides. The chairlike structure has been suggested for the trimers $(H_2GaN_3)_3$ [4,5] and $(Cl_2GaN_3)_3$ [16] in the gas phase; however, $[(CH_3)_2AlN_3]_3$ in solution is a planar Al−N ring (symmetric D_{3h}).[14] The Al_3N_3 cyclic core of the structure represents the basic building block in both cases, but the boatlike structure has not been reported experimentally previously.

As compared to the monomer, the bond lengths of N(α)−Al for the boatlike (1.984, 1.987, and 1.996 Å) and chairlike (1.995 Å) trimers increase by 18.10−19.30 and 19.20 pm, respectively. The N(α)−N(β) bond lengths in the boatlike (1.238 and 1.244 Å) and chairlike (1.239 Å) trimeric structures increase by 2.6−3.2 and 2.7 pm, respectively. The bond lengths of N(β)−N(γ) (1.123 and 1.126 Å) for the boatlike trimer decrease by 0.9−1.2 pm, and the corresponding decrease is 0.9 pm for the chairlike trimer. It can be proposed, based on this evidence, that the bond lengths of the trimer change much more than that of the dimer compared to the monomer. The N−N−N bond angles are about 179.6 and 179.2° for the boatlike and chairlike trimeric structures, respectively. The bond angles for N−N−Al, N−Al−N, and Al−N−Al in the boatlike trimer are about 117.1−119.2, 95.1− 99.1, and 120.9−125.7°, respectively. The corresponding bond angles in the chairlike trimer are 118.7, 98.2, and 121.7°, respectively.

(3.1.4) $(H_2AlN_3)_4$. After the characteristics of $(H_2AlN_3)_2$ and $(H_2AlN_3)_3$ had been examined, the study was extended to $(H_2AlN_3)_4$. Four isomers were found upon geometry optimization with the 6-311+G* basis set, as shown in Figure 4. The tetramer is formed by four Al atoms bridged by the α-nitrogen of the azide groups. They belong to C_s (4A), S_4 (4B), C_i (4C), and C_{4v} (4D) symmetry, respectively. Figure 4A′−D′ structures are the corresponding structures of 4A−D, respectively, with the N_2 portion of the N_3 group also omitted for clarity reasons. Among them, the S_4 symmetry structure with the N_3 alternatively up and down has been suggested for the tetramers $[(CH_3)ClGaN_3]_4$ [17] and $[HClGaN_3]_4$,[18] and they all represent new examples of molecular rings with a cyclooctane-like conformation formed by bridged azides. The other three structures have not been found.

As compared to the monomer, the bond lengths N(α)−Al for the tetramers increase by 16.9− 19.7 pm. The N(α)−N(β) bond lengths in the C_s, S_4, C_i, and C_{4v} symmetry structures increase by 2.8−3.3 pm. The bond lengths N(β)−N(γ) change 0.9−1.2 pm compared to the monomer. The bond angles for N−N−N, N−N−Al, N−Al−N, and Al−N−Al are about 180.0, 117.0−120.0, 100.0−103.0, and 122.0− 126.0°, respectively.

(3.2) Mulliken Charge. The computational Mulliken charge redistribution mainly occurs on the α-N, β-N, and Al atoms in the four-, six-, and eight-membered ring structures. The α-N, N(3), and N(9) atoms both lose 0.0328 e in structure 2A; N(3), N(9), and N(15) atoms in structure 3A lose 2.9681, 1.6844, and 1.6844 e, respectively; N(3) and N(9) atoms in structure 3B both lose 2.2481 e, whereas the N(15) atom acquires 0.1869 e; N(3) and N(15) atoms in structure 4A both lose 2.3682 e, whereas the N(9) and N(21) atoms acquire 0.1283 and 0.1723 e, respectively; four N atoms all lose 2.3976 e in structure 4B; N(3) and (N15) both lose 2.6447 e in structure 4C, and N(9) and N(21) both lose 1.5894 e; N(3) and N(15) both lose 2.2925 e in structure 4D, whereas N(9) and N(21) both acquire 0.2084 e. By a similar analysis, β-N atoms acquire 0.1277−2.4457 e, and Al atoms lose 0.0011− 0.1143 e or acquire 0.0129− 0.0834 e. The charges change is in the following order for the dimer: β-N > Al > α-N atoms; however, for the trimer and tetramer, charge changes are in the order: α-N > β-N > Al atoms.

(3.3) Energy. Table 3 reports the total energies, zero point energies (ZPE), and corrected binding energies obtained at the B3LYP/6-311+G* level. The uncorrected and corrected binding energies are both in the order tetramer > trimer > dimer, 3A

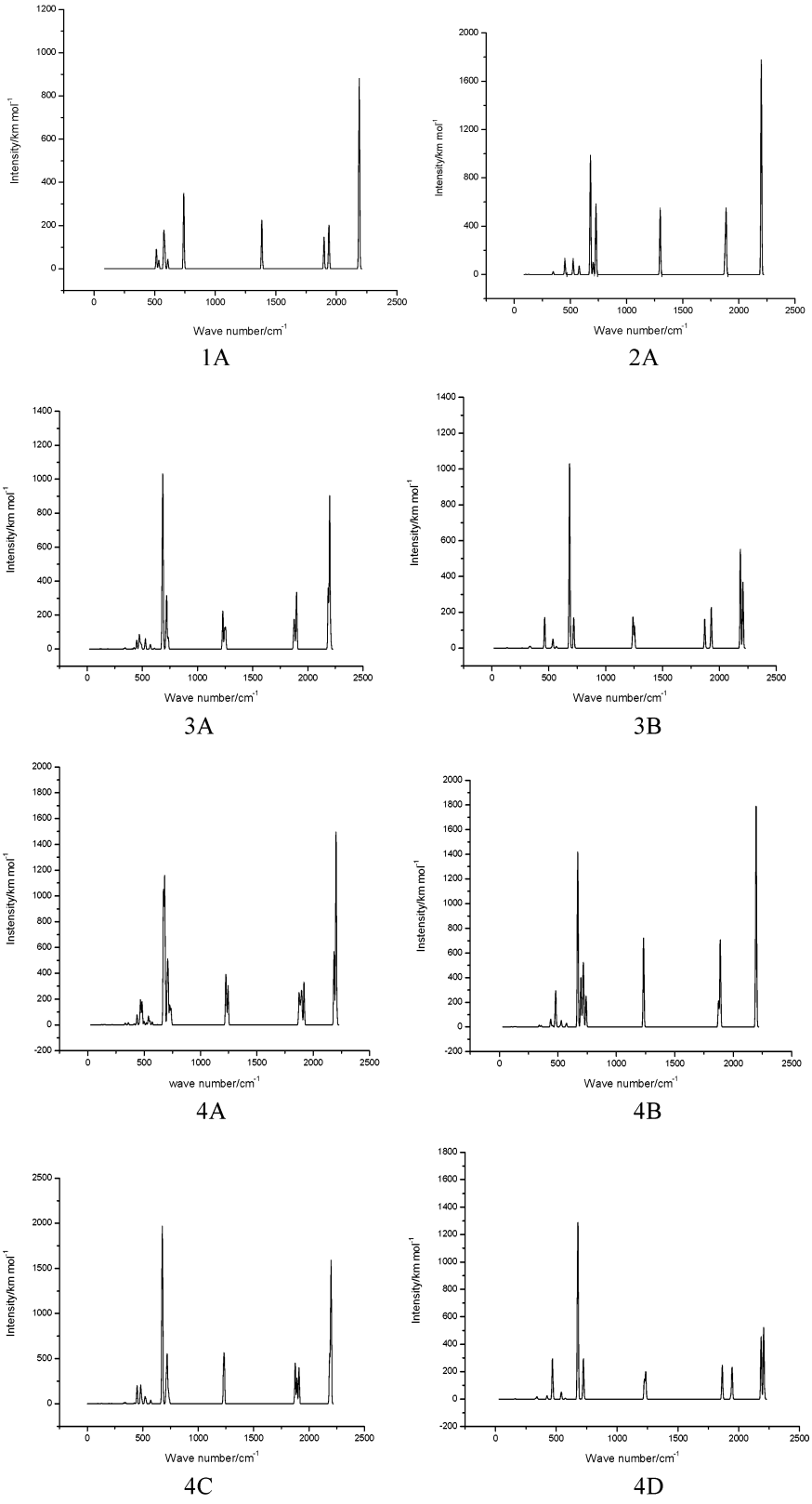

Figure 5. IR spectra of the title compounds.

> 3B, and 4A > 4B > 4C > 4D. The proportions of ZPE corrections to their binding energies ΔE_{ZPEC} are 5.50, 6.04, 5.96, 6.20, 6.32, 6.25, and 6.28% for structures 2A, 3A,B, and 4A−D, respectively, which indicates the ZPE corrections for the binding energies are small. After making the corrections of the ZPE, the binding energies are −166.60, −277.91, −274.21, −379.45, −374.66, −374.05, and −371.67 kJ·mol^{-1} for structures 2A, 3A,B, and 4A−D, respectively. Obviously, the binding energies of the two trimers and the four tetramers are very similar. The binding energy of the lowest energy trimer, possessing C_s symmetry, is about 3.70 kJ·mol^{-1} lower than that of the trimer possessing C_{3v} symmetry. As for the tetramer structures, the changes of binding energies are about 0.61− 7.78 kJ·mol^{-1}. Based on the changes of binding energies upon

TABLE 4: Thermodynamic Properties of H_2AlN_3 Monomer and Its Clusters at Different Temperatures[a]

structures	T (K)	$C_p°$ (J·mol^{-1}·K^{-1})	$S_T°$ (J·mol^{-1}·K^{-1})	$H_T°$ (kJ·mol^{-1})	ΔS_T (J·mol^{-1}·K^{-1})	ΔH_T (kJ·mol^{-1})	ΔG_T (kJ·mol^{-1})
1A	298.2	76.41	300.32	16.22			
	500.0	94.23	344.46	33.61			
	700.0	105.43	378.07	53.65			
2A	298.2	161.04	409.64	29.91	−191.00	−169.13	−112.17
	500.0	202.21	503.76	67.02	−185.16	−166.80	−74.22
	700.0	226.38	575.93	110.05	−180.21	−163.85	−37.70
3A	298.2	246.31	551.93	44.83	−349.03	−281.74	−177.66
	500.0	310.53	696.27	101.74	−337.11	−277.00	−108.45
	700.0	347.55	807.10	167.82	−327.11	−271.04	−42.06
3B	298.2	247.38	535.16	45.05	−365.8	−277.82	−168.74
	500.0	311.04	679.92	102.12	−353.46	−272.92	−96.19
	700.0	347.75	790.86	168.27	−343.35	−266.89	−26.55
4A	298.2	333.29	666.39	60.56	−534.89	−383.77	−224.27
	500.0	419.31	861.48	137.47	−516.36	−376.42	−118.24
	700.0	468.79	1011.05	226.65	−501.23	−367.40	−16.54
4B	298.2	332.96	652.91	60.37	−548.37	−379.17	−215.65
	500.0	419.16	847.87	137.23	−529.97	−371.87	−106.89
	700.0	468.77	997.41	226.40	−514.87	−362.86	−2.45
4C	298.2	333.06	673.22	60.59	−528.06	−378.34	−220.87
	500.0	419.25	868.23	137.47	−509.61	−371.02	−116.22
	700.0	468.82	1017.80	226.65	−494.48	−362.00	−15.86
4D	298.2	333.61	672.71	60.68	−528.57	−375.87	−218.25
	500.0	419.54	867.96	137.66	−509.88	−368.45	−113.51
	700.0	468.88	1017.58	226.87	−494.7	−359.40	−13.11

[a] $\Delta S_T = (S_T°)_i - n(S_T°)_{1A}$, $\Delta H_T = (H_T° + E(\mathrm{HF}) + \mathrm{ZPE})_i - n(H_T° + E(\mathrm{HF}) + \mathrm{ZPE})_{1A}$, $\Delta G_T = \Delta H_T - T\Delta S_T$ (i = 2A, 3A,B, 4A−D with n = 2−4 respectively), and a scale factor of 0.96 for frequencies is imposed.

addition of a new molecule to a cluster, the transition from the trimer to the tetramer involves the same stabilization (about 100.00 kJ·mol^{-1}) as that from the dimer to the trimer.

The corrected binding energies obtained at the B3LYP/6-311++G** and the B3LYP/aug-cc-pVTZ levels are generally close to those obtained with the 6-311+G* basis set. Thus, the use of larger basis sets has no significant influence on the binding energies, which again shows that the 6-311+G* basis set is suitable for the clusters studied here. The calculated corrected binding energy (−198.87 kJ·mol^{-1}) for the dimer at the CCSD(T)/6-311+G* level is lower than that obtained from B3LYP/6-311+G* (−166.60 kJ·mol^{-1}). After making the corrections of the ZPE, the activation energies for the monomer to the dimer conversion are 65.39 and 61.14 kJ·mol^{-1} at the B3LYP/6-311+G* and CCSD(T)/6-311+G* levels, respectively. Obviously the energy barriers are similar at the two levels and are both low, so the dimerization process is very easy.

Inspecting the energies of the highest occupied molecular orbital (HOMO) and the lowest unoccupied molecular orbital (LUMO), that is, E_{HOMO} and E_{LUMO} in Table 3, shows that the E_{HOMO} and E_{LUMO} of structures 1A, 2A, 3A,B, and 4A−D are close, respectively. The energy gaps (E_{gap}) between the E_{HOMO} and E_{LUMO} in all the structures are close, and the magnitudes are 0.21−0.24 au.

(3.4) IR Spectrum. The simulated infrared (IR) spectra for the H_2AlN_3 monomer and its clusters are shown in Figure 5, where the intensity is plotted against the harmonic vibrational frequencies (the scale factor is 0.96 [19]). For the complexity of vibrational modes, it is difficult to assign all bands, so we have only analyzed some vibrational modes that would facilitate assignment of the observed peaks. For the monomer 1A, it is found that N≡N stretching vibrations have the highest intensity and the stretching vibration N═N appears at 1384.32 cm^{-1}. The two peaks at 1938.24 and 1897.92 cm^{-1} are assigned to H−Al−H asymmetric and symmetric stretching vibrational modes, respectively. H−Al−H bending, wagging, and rocking modes are located at 740.16, 576.96, and 514.56 cm^{-1}, respectively. For the dimer 2A, the two N≡N and N═N stretching vibrational modes are calculated at 2199.36 and 1298.88 cm^{-1}, respectively. The peak at 1886.40 cm^{-1} is assigned to H−Al−H asymmetric stretching vibrational modes. H−Al−H bending, wagging, and rocking modes are located at 726.72, 677.76, and 523.2 cm^{-1}, respectively. N≡N and N═N stretching vibrations, H−Al−H asymmetric stretching vibration, bending, and wagging modes for 3A are located at 2198.40, 1228.80, 1897.92, 720.00, and 684.48 cm^{-1}, respectively. The corresponding values for the trimer 3B are 2184.96, 1240.32, 1928.64, 720.00, and 683.52 cm^{-1}. For all the tetramers, N≡N and N═N stretching vibrations, H−Al−H asymmetric stretching vibrational, bending, and wagging modes are located around 2200.00, 1230.00, 1900.00, 720.00, and 675.00 cm^{-1}, respectively.

(3.5) Thermodynamic Properties. Table 4 gives the values of thermodynamic properties of H_2AlN_3 clusters. The magnitudes of heat capacities ($C_p°$) for the clusters with the same number of molecules (n) are approximately the same at each temperature, and larger than $nC_p°$ (1A) by 8.22− 15.52, 17.08−31.46, and 27.32−47.16 J·mol^{-1}·K^{-1} for n = 2, 3, and 4, respectively. The dimerization, trimerization, and tetramerization entropies (ΔS_T) and enthalpies (ΔH_T) decrease from 298.2 to 700.0 K. The dimerization, trimerization, and tetramerization process is therefore an exothermic process accompanied by a decrease in the degree of disorder, and the dimerization, trimerization, and tetramerization become less favored as temperature increases.

The dimerization, trimerization, and tetramerization enthalpies for the most stable structures at 298.2 K and 1 atm are −169.13, −281.74, and −383.77 kJ·mol^{-1}, respectively. Obviously, the transitions from the dimer to the trimer and the trimer to the tetramer involve approximately the same changes of enthalpies (about −100 kJ·mol^{-1}). From the equation $\Delta G = \Delta H - T\Delta S$, we can obtain the change of Gibbs free energy (ΔG). Judged by the value of ΔG_T, the dimerization, trimerization, and tetramerization processes occur spontaneously. Both the values of ΔH_T and ΔG_T imply that the stability sequence is 3A > 3B, which is consistent with results from the corrected binding energy. As for the tetramer, the values of ΔH_T imply that the stability sequence is 4A > 4B > 4C > 4D, which is

consistent with results from the corrected binding energy; however, the values of ΔG_T give the different order 4A > 4C > 4D > 4B. The calculated values of ΔG_T for the formation of the most stable dimer, trimer, and tetramer at 298.2 K are large, which shows that there will be no monomer present. The proportion for 2A:3A:4A is equal to 1.0:12.23:0.63 at 298.2 K. This reveals that the H_2AlN_3 system is involved in dimer−trimer−tetramer equilibria, with the trimer is the main component.

4. Conclusions

The conclusions of this work are as follows:

(1) The DFT/B3LYP method with the 6-311+G* basis set used to calculate H_2AlN_3 clusters consisting of up to four molecules predicts that the clusters all possess cyclic-like structures. The trimer and tetramer possess two and four minima, respectively. Both the structural changes and charge transfers of each cluster are great compared to the monomer.

(2) The binding energies (ca. −274 to −278 kJ·mol^{-1}) of the boatlike and chairlike trimers are similar. The tetramer has several structures that correspond to minima with scarcely different binding energies.

(3) The low activation energy for the monomer to the dimer conversion indicates the dimerization process is very easy.

(4) The ZPE correction is small in all cases.

(5) For the $(H_2AlN_3)_{2-4}$, N≡N and N═N stretching vibrations and H−Al−H asymmetric stretching vibration, bending, and wagging modes are located at 2200.00, 1230.00, 1900.00, 720.00, and 675.00 cm^{-1}, respectively.

(6) The ratio for 2A:3A:4A is equal to 1.0:12.23:0.63 at 298.2 K, which shows that the H_2AlN_3 system is involved in dimer−trimer−tetramer equilibria, with the trimer as the main component.

(7) The relative energies and other computed properties will change at the multireference level.

Acknowledgment. This project was supported by the National Natural Science Foundation of China (Grant No. 20173028).

References and Notes

(1) Boyd, D. C.; Haasch, R. T.; Mantell, D. R.; Schulze, R. K.; Evans, J. F.; Gladfelter, W. L. *Chem. Mater.* **1989**, *1*, 119.

(2) Boo, J. H.; Lee, S. B.; Kim, Y. S.; Park, J. T.; Yu, K. S.; Kim, Y. *Phys. Status Solidi A* **1999**, *176*, 711.

(3) Sheppard, L. M. *Am. Ceram. Soc. Bull.* **1990**, *69*, 1801.

(4) McMurran, J.; Dai, D.; Balasubramanian, K.; Steffek, C.; Kouvetakis, J.; Hubbard, J. L. *Inorg. Chem.* **1998**, *37*, 6638.

(5) McMurran, J.; Kouvetakis, J.; Smith D. J. *Appl. Phys. Lett.* **1999**, *74*, 883.

(6) Fletcher, R.; Powell, M. J. D. *Comput. J.* **1963**, *6*, 163.

(7) Schlegel, H. B. *J. Comput. Chem*. **1982**, *3*, 214.

(8) Peng, C. Y.; Ayala, P. Y.; Schlegel, H. B.; Frisch, M. J. *J. Comput. Chem.* **1996**, *17*, 49.

(9) Lee, E. P. F.; Dyke, J. M.; Claridge, R. P. *J. Phys. Chem. A* **2002**, *106*, 8680.

(10) Frisch, M. J.; Trucks, G. W.; Schlegel, H. B.; Scuseria, G. E.; Robb, M. A.; Cheeseman, J. R.; Zakrzewski, V. G.; Montgomery, J. A.; Stratmann, R. E.; Burant, J. C.; Dapprich, S.; Millam, J. M.; Daniels, A. D.; Kudin, K. N.; Strain, M. C.; Farkas, O.; Tomasi, J.; Barone, V.; Cossi, M.; Cammi, R.; Mennucci, B.; Pomelli, C.; Adamo, C.; Clifford, S.; Ochterski, J.; Petersson, G. A.; Ayala, P. Y.; Cui, Q.; Morokuma, K.; Malick, D. K.; Rabuck, A. D.; Raghavachari, K.; Foresman, J. B.; Cioslowski, J.; Ortiz, J. V.; Stefanov, B. B.; Liu, G.; Liashenko, A.; Piskorz, P.; Komaromi, I.; Gomperts, R.; Martin, R. L.; Fox, D. J.; Keith, T.; Al-Laham, M. A.; Peng, C. Y.; Nanayakkara, A.; Gonzalez, C.; Challacombe, M.; Gill, P. M. W.; Johnson, B. G.; Chen, W.; Wong, M. W.; Andres, J. L.; Head-Gordon, M.; Replogle, E. S.; Pople, J. A. *Gaussian 98*, Revision A.7; Gaussian Inc.: Pittsburgh, PA, 1998.

(11) Dehnicke, K.; Kruger, N. *Z. Anorg. Allg. Chem.* **1978**, *444*, 71.

(12) Steffek, C.; McMurran, J.; Pleune, B.; Kouvetakis, J. *Inorg. Chem.* **2000**, *39*, 1615.

(13) Fischer, R. A.; Sussek, H.; Miehr, A.; Pritzkow, H.; Herdtweck, E. *J. Organomet. Chem.* **1997**, *548*, 73.

(14) Müller, J.; Dehnicke, K. *J. Organomet. Chem.* **1968**, *12*, 37.

(15) Kim, J.; Bott, S. G.; Hoffman, D. M. *Inorg. Chem.* **1998**, *37*, 3835.

(16) McMurran, J.; Todd, M.; Kouvetakis, J. *Appl. Phys. Lett.* **1996**, *69*, 203.

(17) Kouvetakis, J.; McMurran, J.; Steffek, C.; Groy, T. L.; Hubbard, J. L. *Inorg. Chem.* **2000**, *39*, 3805.

(18) McMurran, J.; Kouvetakis, J.; Nesting, D. C.; Smith, D. J.; Hubbard, J. L. *J. Am. Chem. Soc.* **1998**, *120*, 5233.

(19) Pople, J. A.; Schlegel, H. B.; Krishnan, R.; Defrees, D. J.; Binkley, J. S.; Frisch, M. J.; Whiteside, R. A.; Hout, R. F.; Hehre, W. J. *Int. J. Quantum Chem., Quantum Chem. Symp.* **1981**, *15*, 269.